

Modelling Solar Oscillation Power Spectra: III. Spatiotemporal spectra of solar granulation velocity field as seen in SDO HMI Doppler-velocity measurements

SERGEI V. VORONTSOV,^{1,2} STUART M. JEFFERIES,³ AND TIMOTHY P. LARSON⁴

¹*Astronomy Unit, School of Physical and Chemical Sciences, Queen Mary University of London, Mile End Road, London E1 4NS, UK*

²*Institute of Physics of the Earth, B. Gruzinskaya 10, Moscow 123810, Russia*

³*Department of Physics and Astronomy, Georgia State University, Atlanta, GA, USA*

⁴*tplarson@sun.stanford.edu*

ABSTRACT

We suggest a physically motivated model of the uncorrelated background, which can be used to improve the accuracy of helioseismic frequency measurements **when the background contributes significantly to the formation of spectral lines of acoustic resonances**. The basic assumption of our model is that the correlation length of the convective motions is small compared with horizontal wavelength R_{\odot}/ℓ of the observations, where ℓ is the degree of spherical harmonic $Y_{\ell m}(\theta, \varphi)$. When applied to solar power spectra at frequencies below acoustic resonances, the model reveals a distinct sensitivity to solar rotation: advection of the convective velocity pattern brings spatial correlations in the apparent stochastic velocity field (temporal correlations in the co-rotating frame induce spatial correlations in the inertial frame). The induced spatiotemporal correlations manifest themselves as an antisymmetric component in the dependence of the convective noise power on azimuthal order m , which allows us to address the solar differential rotation. With 360 days of data obtained by the Helioseismic and Magnetic Imager onboard the Solar Dynamics Observatory, we measure three components of the rotation rate as function of latitude using only $\ell = 300$. This result indicates that the model suggests a new way of measuring solar subsurface rotation. This approach can complement traditional measurements based on correlation tracking.

Keywords: methods: data analysis — Sun: helioseismology — Sun: oscillations— Sun: rotation— Sun: convection

1. INTRODUCTION

The most challenging task in contemporary helioseismology is to reduce systematic errors in estimating solar p-mode frequencies. This problem is most prominent when analyzing long timeseries, which are expected to have the smallest random errors. A large amount of data accumulated over the decades in dedicated ground-based and space projects calls for significant improvements to the data analysis pipeline to exploit their full diagnostic potential. For a recent account of the available data and its processing, we refer the reader to [Larson & Schou \(2015, 2018\)](#) and [Korzennik \(2005, 2023\)](#).

Multiple sources of potential systematic errors come into play when we attempt to measure an oscillation frequency with accuracy better than the width of its resonant line in the observed power spectrum. Systematic offsets are caused by inadequate modeling of the asymmetric line profile, inaccurate treatment of nearby spatial leaks, and incorrect magnitude and/or frequency gradient of the uncorrelated background noise. Spatial leaks are characterized by the so-called leakage matrix, and themselves subject to approximations regarding instrumental and optical distortions and mode-coupling effects.

This study is focused on global modeling of the uncorrelated background. It is common practice in the mode-fitting procedures to account for the uncorrelated background with a single free parameter for each (n, ℓ) frequency multiplet to ensure numerical stability. When dependence on azimuthal order m is allowed, it is evaluated in a small frequency interval in the vicinity of resonances, an interval typically contaminated by spatial leaks. We are seeking a description of the background in the entire range of (n, ℓ, m) by fitting a single slowly-varying function of frequency only.

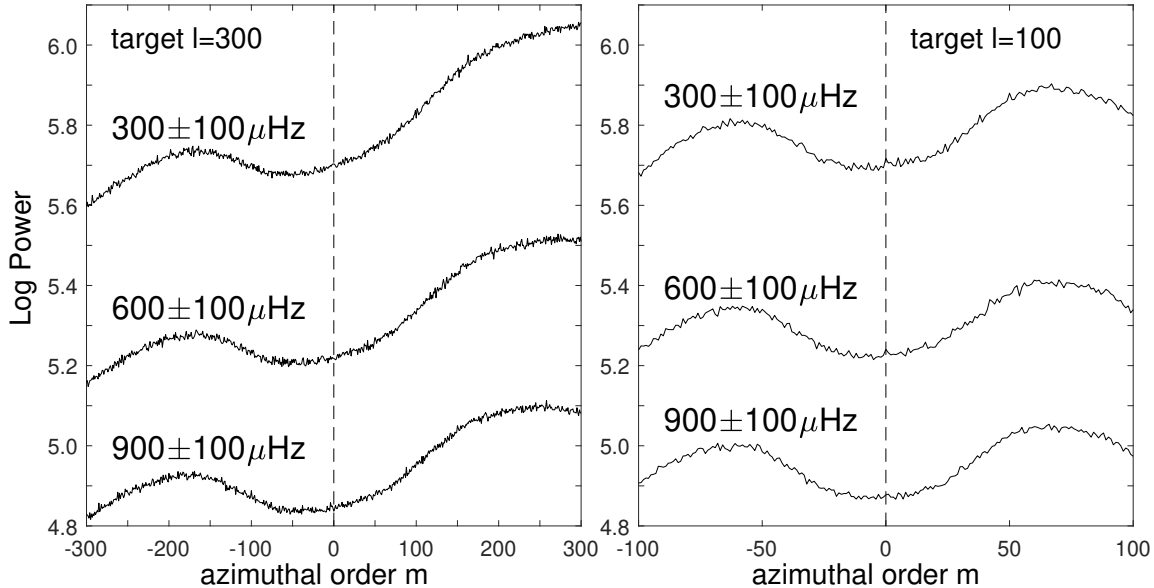


Figure 1. Observational noise power as function of azimuthal order m at $\ell = 300$ (left) and $\ell = 100$ (right) measured at frequencies around $300\mu\text{Hz}$, $600\mu\text{Hz}$ and $900\mu\text{Hz}$.

42 It is natural to examine noise power in a frequency range below 1mHz , where global oscillation resonances are
 43 buried below the noise level. This study analyzes power spectra obtained from a **360 day-long time-series of**
 44 **Dopplergrams measured with Helioseismic and Magnetic Imager (HMI) onboard the Solar Dynamics**
 45 **Observatory (SDO)**. Our timeseries begins on 2019.03.14 and covers the one-year period synced with HMI's regular
 46 72 day global processing cadence and that is most closely centered on solar activity minimum. Figure 1 shows the
 47 observed power at degree $\ell = 300$ and $\ell = 100$ as a function of m at frequencies around $300\mu\text{Hz}$, $600\mu\text{Hz}$ and $900\mu\text{Hz}$;
 48 the measurements were averaged over $\pm 100\mu\text{Hz}$ frequency intervals.

49 We can make two interesting observations:

50 (i) For each of two values of degree ℓ , the three curves obtained at frequencies that differ by a factor three are
 51 essentially the same; the only difference is a nearly-uniform vertical shift on the logarithmic scale. This feature
 52 indicates that the functional dependence of the noise power on the spatial spectral numbers (ℓ, m) and temporal
 53 frequency ω is separable; and

54 (ii) the dependence on m is highly asymmetric. This feature points immediately to the effects of solar rotation, as
 55 the instrument's sensitivity does not depend on the sign of m . With our sign convention, harmonics with positive
 56 m are prograde waves, i.e., waves moving in the direction of rotation. In the co-rotating frame, these waves have a
 57 smaller frequency, and we see they have higher noise.

58 Below is our attempt to understand this behavior in detail. We assume that the noise comes from the turbulent
 59 convective velocity field in the solar photosphere. In Section 2, we analyze the spectral measures of this noise,
 60 assuming that the correlation length of the convective motions is small compared with observational wavelength
 61 R_{\odot}/ℓ . We consider in detail the effects of differential rotation. Section 3 describes its measurement from the odd
 62 (in m) component of the noise power in SDO HMI measurements. We also analyze the even (in m) component,
 63 governed by different sensitivity of the instrument to different spatial harmonics of the velocity field. Extension of the
 64 leakage-matrix computations to include the instrument's response to torsional components of the velocity field, which
 65 enter the analysis, is described in the Appendix. Section 4 suggests an initial approximation for the noise power in
 66 the frequency interval containing acoustic resonances, which has to be iteratively improved when fitting solar power
 67 spectra in frequency measurements. Our results are discussed in Section 5.

68 2. SPECTRAL MEASURES OF GRANULATION VELOCITY FIELD IN SPATIAL AND TEMPORAL 69 DOMAINS

We work in a spherical coordinate system (r, θ, φ) aligned with solar rotation axis, and expand the time-dependent surface velocity field $\mathbf{v}(\theta, \varphi, t)$ in vector spherical harmonics as

$$\mathbf{v}(\theta, \varphi, t) = \sum_{\ell, m} [u_{\ell m}(t) \hat{r} Y_{\ell m}(\theta, \varphi) + v_{\ell m}(t) \nabla_1 Y_{\ell m}(\theta, \varphi) - w_{\ell m}(t) \hat{r} \times \nabla_1 Y_{\ell m}(\theta, \varphi)] \quad (1)$$

where ∇_1 is the angular part of gradient operator, $\nabla_1 = \hat{\theta} \partial / \partial \theta + \sin^{-1} \theta \hat{\varphi} \partial / \partial \varphi$, and hats designate unit vectors. We make a Fourier transform of the time string of some large length T

$$\int_0^T e^{i\omega t} \mathbf{v}(\theta, \varphi, t) dt = \sum_{\ell, m} [U_{\ell m}(\omega) \hat{r} Y_{\ell m}(\theta, \varphi) + V_{\ell m}(\omega) \nabla_1 Y_{\ell m}(\theta, \varphi) - W_{\ell m}(\omega) \hat{r} \times \nabla_1 Y_{\ell m}(\theta, \varphi)]. \quad (2)$$

Using orthogonality properties of vector spherical harmonics

$$\int_{4\pi} [\nabla_1 Y_{\ell m}^*(\theta, \varphi)] \cdot [\nabla_1 Y_{\ell' m'}(\theta, \varphi)] d\varpi = \int_{4\pi} [-\hat{r} \times \nabla_1 Y_{\ell m}^*(\theta, \varphi)] \cdot [-\hat{r} \times \nabla_1 Y_{\ell' m'}(\theta, \varphi)] d\varpi = \ell(\ell+1) \delta_{\ell' \ell} \delta_{m' m}, \quad (3)$$

where star designates complex conjugate **and** ϖ is solid angle, we have

$$U_{\ell m}(\omega) = \int_0^T e^{i\omega t} u_{\ell m}(t) dt = \int_0^T e^{i\omega t} dt \int_{4\pi} \mathbf{v}(\theta, \varphi, t) \cdot \hat{r} Y_{\ell m}^*(\theta, \varphi) d\varpi, \quad (4)$$

$$\ell(\ell+1) V_{\ell m}(\omega) = \int_0^T e^{i\omega t} v_{\ell m}(t) dt = \int_0^T e^{i\omega t} dt \int_{4\pi} \mathbf{v}(\theta, \varphi, t) \cdot \nabla_1 Y_{\ell m}^*(\theta, \varphi) d\varpi, \quad (5)$$

$$\ell(\ell+1) W_{\ell m}(\omega) = \int_0^T e^{i\omega t} w_{\ell m}(t) dt = \int_0^T e^{i\omega t} dt \int_{4\pi} \mathbf{v}(\theta, \varphi, t) \cdot [-\hat{r} \times \nabla_1 Y_{\ell m}^*(\theta, \varphi)] d\varpi. \quad (6)$$

These expressions are obtained by taking scalar product of both sides of Equation (1) with $\hat{r} Y_{\ell m}^*(\theta, \varphi)$, $\nabla_1 Y_{\ell m}^*(\theta, \varphi)$, and $-\hat{r} \times \nabla_1 Y_{\ell m}^*(\theta, \varphi)$, integrating in angular coordinates and taking the Fourier transform.

We assume $\mathbf{v}(\theta, \varphi, t)$ to be a particular realization of a stationary stochastic process with zero mean. Quantities in the left-hand sides of Equations (4-6), represented by stochastic integrals in the right-hand sides, are thus random variables with zero mean, $E[U_{\ell m}(\omega)] = E[V_{\ell m}(\omega)] = E[W_{\ell m}(\omega)] = 0$. We are interested in evaluating their variances $\text{Var} U_{\ell m}(\omega) = E[U_{\ell m}(\omega)^* U_{\ell m}(\omega)]$, $\text{Var} V_{\ell m}(\omega)$ and $\text{Var} W_{\ell m}(\omega)$, together with non-zero covariances, if any.

We associate $\mathbf{v}(\theta, \varphi, t)$ with the turbulent velocity field of convective motions imposed on a stationary large-scale background flow produced by differential rotation and meridional circulation. The basic assumption of our model is that for an observer moving together with the background flow, the convective velocities do not correlate in space. For the granulation velocity field, this assumption can only be valid in a limited range of harmonic degree ℓ , that is where a typical size of a granule is small compared with the horizontal wavelength R_{\odot}/ℓ . Here, we consider power spectra in the range $0 \leq \ell \leq 300$, and limit our analysis to the background flow produced by differential rotation only: the effects of meridional circulation require a different treatment and will be left for further studies.

To make derivations more transparent, we consider a model with the effects of rotation discarded before generalizing the results to include the effects of solid-body rotation and then differential rotation.

(i) *Non-rotating Sun*. Changing the order of integration, we rewrite Equation (4) as

$$U_{\ell m}(\omega) = \int_{4\pi} Y_{\ell m}^*(\theta, \varphi) \tilde{v}_r(\theta, \varphi, \omega) d\varpi, \quad (7)$$

where $\tilde{v}_r(\theta, \varphi, \omega)$ is the Fourier transform of radial velocity, $\tilde{v}_r(\theta, \varphi, \omega) = \int_0^T e^{i\omega t} v_r(\theta, \varphi, t) dt$, and consider the covariance

$$\text{Cov} [U_{\ell m}(\omega), U_{\ell' m'}(\omega)] = E \left[\int_{4\pi} Y_{\ell m}(\theta, \varphi) \tilde{v}_r^*(\theta, \varphi, \omega) d\varpi \cdot \int_{4\pi} Y_{\ell' m'}^*(\theta, \varphi) \tilde{v}_r(\theta, \varphi, \omega) d\varpi \right]. \quad (8)$$

Considering the first integral on the right-hand side as a sum of integrals over small angular areas $\Delta\varpi_i$ and likewise for the second integral indexed by j , we notice that the result is only nonzero for diagonal elements $i = j$; the expectation value of the cross-terms is zero because the \tilde{v}_r -values are not correlated in space. We also know that the variance has

107 an additive property. Therefore, if we replace the entire integration domain 4π in the right-hand side of Equation (8)
108 by a small angular element $\Delta\varpi$, the result will be proportional to $\Delta\varpi$. We thus have

$$109 \quad \text{Cov}[U_{\ell m}(\omega), U_{\ell' m'}(\omega)] = \int_{4\pi} Y_{\ell m}(\theta, \varphi) Y_{\ell' m'}^*(\theta, \varphi) \sigma_r^2(\omega) d\varpi = \delta_{\ell' \ell} \delta_{m' m} \sigma_r^2(\omega), \quad (9)$$

110 where

$$111 \quad \sigma_r^2(\omega) = \lim_{\Delta\varpi \rightarrow 0} \frac{1}{\Delta\varpi} \mathbb{E} \left[\int_{\Delta\varpi} \tilde{v}_r^*(\theta, \varphi) \tilde{v}_r(\theta, \varphi) d\varpi \right] \quad (10)$$

112 is positive spectral measure of the variance of vertical velocities, which we assume to be uniform over the solar surface.

113 We work in a similar manner with the contribution from the horizontal components of the velocity field, $v_\theta(\theta, \varphi, t)$
114 and $v_\varphi(\theta, \varphi, t)$, which have corresponding Fourier transforms $\tilde{v}_\theta(\theta, \varphi, \omega)$ and $\tilde{v}_\varphi(\theta, \varphi, \omega)$. We assume that horizontal
115 velocities are isotropic in azimuthal direction and, therefore, the two orthogonal horizontal components do not correlate
116 with each other and

$$117 \quad \sigma_\theta^2(\omega) = \sigma_\varphi^2(\omega) = \frac{1}{2} \sigma_h^2(\omega), \quad (11)$$

118 where $\sigma_h^2(\omega)$ is spectral measure of absolute values of horizontal velocities. The result is

$$119 \quad \text{Cov}[V_{\ell m}(\omega), V_{\ell' m'}(\omega)] = \text{Cov}[W_{\ell m}(\omega), W_{\ell' m'}(\omega)] = \frac{1}{2\ell(\ell+1)} \delta_{\ell' \ell} \delta_{m' m} \sigma_h^2(\omega), \quad (12)$$

120 where we note that at $\ell = 0$, the horizontal components are identically zero.

121 We expect no correlation between U , V and W because of the orthogonality of corresponding velocity components
122 and symmetry considerations. To see this, let \mathbf{v} be velocity vector at a particular point on the solar surface, with
123 $v_r = v \cdot \hat{r} Y_{\ell m}(\theta, \varphi)$ and $v_h = v \cdot \nabla_1 Y_{\ell' m'}(\theta, \varphi)$. From geometrical considerations, the joint probability density function
124 $p(v_r, v_h)$ is symmetric in v_h , i.e. for any value of v_r , two events with v_h of the same magnitude but of opposite sign
125 have the same probability. The expectation value of their product $\mathbb{E}(v_r v_h) = 0$, and hence there is no correlation
126 between $U_{\ell m}$ and $V_{\ell' m'}$. The same arguments apply to correlations between U and W and between V and W .

127 We now extend the analysis to include the effects of rotation.

128 (ii) *Solid-body rotation.* In this scenario, the Sun rotates with uniform angular velocity Ω in the observational frame.
129 **The effect of Coriolis forces on the velocity field at the scale of solar granulation is expected to be**
130 **smeared away by spatial averaging**, so we can assume that in the co-rotating frame, the **observable statistical**
131 **properties of** convective motions are not influenced by rotation. When the convective velocity field is observed in
132 another reference frame, the only change is due to advection: in the spherical-harmonic decomposition, a component
133 of azimuthal order m will have its temporal frequency shifted by $m\Omega$. The net result is that $\sigma_r^2(\omega)$ in Equation (9)
134 has to be replaced with $\sigma_r^2(\omega - m\Omega)$, and similar with $\sigma_h^2(\omega)$ in Equation (12).

135 (iii) *Differential rotation.* We now allow the rotation to change with latitude. When the rotation is uniform, the
136 variance of $U_{\ell m}(\omega)$ can be written as

$$137 \quad \text{Var} U_{\ell m}(\omega) = \frac{2\ell+1}{2} \frac{(\ell-m)!}{(\ell+m)!} \int_{-1}^1 [P_\ell^m(z)]^2 \sigma_r^2(\omega - m\Omega) dz, \quad z = \cos \theta. \quad (13)$$

138 Since contributions to the variance coming from different latitudes simply add up, the same expression will be valid
139 when Ω in the right-hand side is allowed to depend on latitude, **meaning we can divide the spherical surface**
140 **into thin latitudinal belts with each one in its own co-rotating frame.** We will assume now that the rotation
141 is slow; limiting the analysis to terms linear in Ω ,

$$142 \quad \sigma_r^2(\omega - m\Omega(z)) = \sigma_r^2(\omega) - m \frac{d\sigma_r^2}{d\omega} \Omega(z), \quad (14)$$

143 and hence

$$144 \quad \begin{aligned} \text{Var} U_{\ell m}(\omega) &= \sigma_r^2(\omega) - m \frac{d\sigma_r^2}{d\omega} \frac{2\ell+1}{2} \frac{(\ell-m)!}{(\ell+m)!} \int_{-1}^1 [P_\ell^m(z)]^2 \Omega(z) dz \\ &= \sigma_r^2 \left(\omega - m \frac{2\ell+1}{2} \frac{(\ell-m)!}{(\ell+m)!} \int_{-1}^1 [P_\ell^m(z)]^2 \Omega(z) dz \right), \end{aligned} \quad (15)$$

where $P_\ell^m(z)$ are associated Legendre polynomials.

Following an approach which is standard in solar seismology, we represent $\Omega(z)$ by an expansion

$$\Omega(z) = \sum_{s=1,3,5,\dots} \Omega_s \frac{dP_s(z)}{dz}, \quad (16)$$

where $P_s(z)$ are Legendre polynomials. Note that only even components of $\Omega(z)$ enter our result, as $[P_\ell^m(z)]^2$ is even function of z .

The required angular integrals are

$$\begin{aligned} m \frac{2\ell+1}{2} \frac{(\ell-m)!}{(\ell+m)!} \int_{-1}^1 [P_\ell^m(z)]^2 \frac{dP_s(z)}{dz} dz &= (-1)^{k+1} \frac{(\ell-1)!}{(\ell-k)!} \frac{(2\ell+1)!!}{(2\ell+2k-1)!!} \frac{(2k-1)!!}{(k-1)!} \mathcal{P}_{2k-1}^{(\ell)}(m) \\ &= \left(\frac{4\pi}{2s+1} \right)^{1/2} \gamma_{s\ell}^m, \end{aligned} \quad (17)$$

where $s = 2k - 1$, $\gamma_{s\ell}^m$ are odd polynomials of degree s in m defined in (Ritzwoller & Lavelly 1991) and $\mathcal{P}_{2k-1}^{(\ell)}(m)$ are polynomials currently used in solar seismology to describe frequency splittings of solar oscillations, following normalization defined in (Schou et al. 1994). Equation (17) can be derived by expanding $dP_s(z)/dz$ in $P_i(z)$, $i < s$, and evaluating integrals of triple products of Legendre polynomials. Convenient recurrence relations for evaluating $\mathcal{P}_{2k-1}^{(\ell)}(m)$ can be found in (Vorontsov 2007). We thus have

$$\text{Var } U_{\ell m}(\omega) = \sigma_r^2 \left[\omega - \sum_{s=1,3,\dots} \left(\frac{4\pi}{2s+1} \right)^{1/2} \gamma_{s\ell}^m \Omega_s \right]. \quad (18)$$

Introducing a -coefficients, commonly used in solar seismology, we have

$$\text{Var } U_{\ell m}(\omega) = \sigma_r^2 \left(\omega - \sum_{s=1,3,\dots} 2\pi a_s \mathcal{P}_s^{(\ell)}(m) \right). \quad (19)$$

The relation between the expansion coefficients Ω_s and a_s is provided by Equation (17); in particular,

$$2\pi a_1 = \Omega_1, \quad 2\pi a_3 = -\frac{3(\ell-1)}{(2\ell+3)} \Omega_3, \quad 2\pi a_5 = \frac{15(\ell-1)(\ell-2)}{2(2\ell+3)(2\ell+5)} \Omega_5. \quad (20)$$

Variances of $V_{\ell m}(\omega)$ and $W_{\ell m}(\omega)$ (Equations 5, 6) are transformed by the effects of differential rotation in precisely the same way.

We have an interesting observation: under the effects of differential rotation, each spectral component of velocity variances 'split' in its observed frequency in precisely the same way as an undistorted frequency of solar oscillations would split under the effects of the same differential rotation if the influence of Coriolis forces can be discarded (leaving effects of advection only) and differential rotation does not change with depth.

We also note that the possible inaccuracy, introduced by linearization in the rotation rate (Equations 14, 15) can only affect the response to differential components. The response to the dominant Ω_1 -component is treated correctly whatever its magnitude, because $(4\pi/(2s+1))^{1/2} \gamma_{s\ell}^m = m$ for $s = 1$.

3. SOLAR CONVECTIVE VELOCITY FIELD AS SEEN IN SDO HMI POWER SPECTRA

Instrumental response to different velocity field components does not depend on the sign of the azimuthal order m . Parameters of differential rotation (Equations 19, 20) can thus be calculated by shifting in frequency the power spectra of individual orders m to eliminate the odd (in m) component of the noise power. This procedure was implemented iteratively to account for a finite frequency window ($\pm 100\mu\text{Hz}$ in our measurement). The result obtained at $\ell = 300$ at frequencies around $900\mu\text{Hz}$ is $a_1 = 390.0 \pm 0.9$ nHz (synodic), $a_3 = 20.0 \pm 1.3$ nHz, and $a_5 = 2.4 \pm 1.7$ nHz. Corresponding coefficients of the polynomial expansion of the angular rotation rate (Equation 16) are thus $\Omega_1/(2\pi) = a_1$, $\Omega_3/(2\pi) = -13.4 \pm 0.9$ nHz, and $\Omega_5/(2\pi) = 1.3 \pm 0.9$ nHz. **To evaluate the quality of this fit,**

we use a merit function defined as the rms value of the residuals weighted with the observational uncertainties, which are evaluated under the standard assumption that observational power in an individual frequency channel has a χ^2 -distribution with two degrees of freedom. Ideally, the value of this merit function should be close to one. In our measurement, it is 1.073, which indicates that the targeted odd (in m) component is successfully eliminated in the 'de-rotated' power spectra.

This result should be compared with other available measurements. Helioseismic measurements of solar internal rotation lose their accuracy in the sub-surface layers, where the rotation varies rapidly with depth, and global modes lose their resolving power. However, the measurements reduced to solar activity minimum (Figure 8 of Vorontsov et al. 2002) indicate the surface values of $\Omega_1/(2\pi) \simeq 435$ nHz (sidereal, or synodic plus 31.6 nHz), $\Omega_3/(2\pi) \simeq -13$ nHz and $\Omega_5/(2\pi) \simeq 1$ nHz. The mean rotation rate $\Omega_1/(2\pi)$ inferred from the convective noise is thus about 13 nHz slower; Ω_3 and Ω_5 appear to be in perfect agreement.

A classical result of measuring solar differential rotation using correlation tracking (Snodgrass & Ulrich 1990) is

$$\Omega/(2\pi) = 0.473 - 0.077 \cos^2 \theta - 0.0575 \cos^4 \theta \text{ } (\mu\text{Hz}) \quad (21)$$

sidereal, which translates to $\Omega_1/(2\pi) = 468.0$ nHz sidereal, $\Omega_3/(2\pi) = -5.15$ nHz and $\Omega_5/(2\pi) = -1.46$ nHz. The difference between our measurement and this result is much bigger. One realistic scenario is that the measurements refer to different effective depths below the visible solar surface. Still, the result of Snodgrass & Ulrich (1990) is hard to reconcile with the results of our earlier helioseismic measurements (e.g., Vorontsov et al. 2002), where $\Omega_3/(2\pi) \simeq -14 \pm 1$ nHz was found to be nearly constant with depth over the entire convective envelope, and $\Omega_1/(2\pi)$ was found to increase with depth to a maximum value of about 449 nHz (sidereal) at a depth of about 6 percent of solar radius.

Our measurement of the rotation of the solar granulation pattern requires a certain level of data quality. It benefits from going to higher degree ℓ (wider range of azimuthal orders m), from observations with better spatial resolution (spatial leaks are not accounted for in the rotation measurement), and from observations of longer duration (better signal-to-noise ratio). When using 360d SDO HMI data, the measurement of relatively small differential components of the rotation rate loses stability at degrees ℓ less than about 200, leaving the possibility of evaluating mean rotation only. This precludes the use of data from the Global Oscillation Network Group (GONG), because they only provide spherical harmonic timeseries up to $\ell = 200$.

Power spectra up to $\ell = 300$ are indeed available from the Structure Program of the Michelson Doppler Imager (MDI) onboard the Solar and Heliospheric Observatory (SOHO), but even these are unsuitable for measuring the differential components of the rotation due to contamination by spatial leaks resulting from insufficient spatial resolution and gaussian smoothing.

We have attempted a measurement identical to that described above at $\ell = 300$ but using 63 days of data taken by the Dynamics Program of SOHO MDI in 1996, which have much higher resolution than the Structure data. The result is $a_1 = 374.3 \pm 2.2$ nHz and $a_3 = 20.1 \pm 3.1$ nHz, where a_5 could not be determined due to the shorter length of observation. While the a_3 coefficient is in agreement with the HMI measurement, the a_1 coefficient appears to be about 16 nHz smaller. We conjecture that the difference comes from contamination of the MDI power spectra with bigger spatial leaks due to a smaller spatial resolution of the instrument. This explanation is confirmed by analyzing SDO HMI power spectra obtained with artificially degraded spatial resolution (Larson & Schou 2018). Some of the difference may also be attributed to the different height of formation of the spectral lines used by the two instruments: SOHO MDI was observing the Sun slightly higher in the atmosphere (Fleck et al. 2011).

With the odd (in m) component successfully eliminated in the properly "de-rotated" observational power spectra, we now analyze the remaining even component. For the same measurement at $\ell = 300$ and frequencies $900 \pm 100 \mu\text{Hz}$, this component is shown by a thin line in Figure 2, where the remaining even component of the observed power

$$B_{\ell m}^2(\omega) = B_{\ell}^2(m) \overline{B}^2(\omega) \quad (22)$$

is represented by the dimensionless variable $B_{\ell}^2(m)$ in units of $\overline{B}^2(\omega)$, which is the m -averaged value of $B_{\ell m}^2(\omega)$.

The contribution of the convective velocity field to the observational power spectra comes through multiple $U_{\ell m}$, $V_{\ell m}$ and $W_{\ell m}$ -components (Equations 4-6). As these components do not correlate with each other, we have, for the

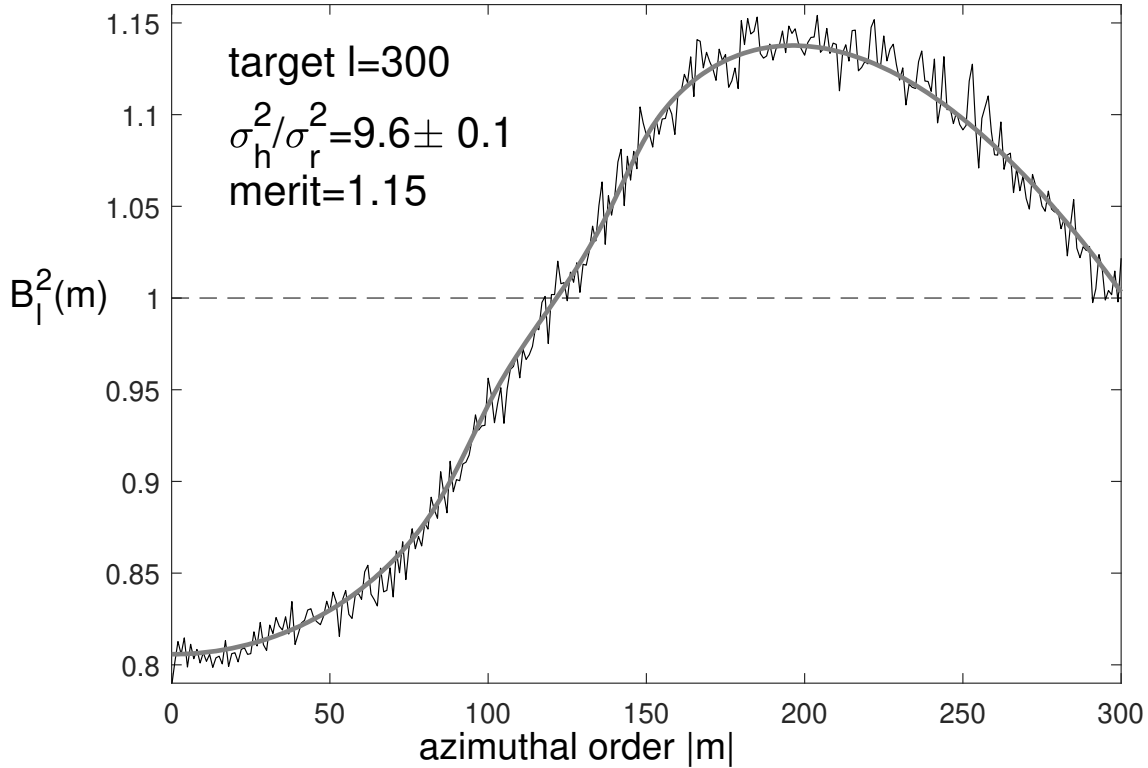


Figure 2. Even component in the observational noise power as function of azimuthal order m at $l = 300$ measured at frequencies around $900\mu\text{Hz}$ (thin line). Thick gray line shows its approximation obtained by fitting synthetic power.

231 'de-rotated' power spectra,

$$232 \quad B_{\ell m}^2(\omega) = \sigma_r^2(\omega) \sum_{\ell' m'} |R_{\ell' \ell}^{m' m}|^2 + \frac{\sigma_h^2(\omega)}{2\ell(\ell+1)} \left[\sum_{\ell' m'} |H_{\ell' \ell}^{m' m}|^2 + \sum_{\ell' m'} |T_{\ell' \ell}^{m' m}|^2 \right], \quad (23)$$

233 where we introduce the notation R , H , and T to designate separate leakage matrices which specify sensitivity coefficients
 234 of the instrument to radial components of the velocity field, horizontal components of the poloidal vector fields, and
 235 components of the toroidal fields (Equation 1), respectively. To make sure that a sufficient amount of spectral leaks
 236 are accounted for, the leakage matrices were computed with ℓ' in the range $\ell \pm 30$ and m' in the range $m \pm 30$.
 237 Computation of the leakage matrices followed a semi-analytic approach described in (Vorontsov & Jefferies 2005),
 238 which was generalized to include the instrument's response to toroidal velocity fields; details can be found in the
 239 Appendix. To account for a finite resolution of the instrument in the CCD plane, the leakage-matrix analysis involves
 240 convolution of the images with a 2D Gaussian point-spread function (PSF). When working with high-resolution HMI
 241 data in the intermediate-degree range $\ell \leq 300$, the width of the PSF was set to zero, meaning infinite resolution, or a
 242 PSF described by 2D Dirac δ -function. The solar B-angle was set to 5.11° , the rms value of its annual variation (for
 243 a small B-angle, its effect on the leakage-matrix elements is quadratic in its magnitude).

244 The observed power $B_{\ell m}^2(\omega)$ considered as a function of m at $\ell = 300$ is fitted by a linear combination of the two
 245 terms in the right-hand side of Equation (23) with unknown coefficients σ_r^2 and σ_h^2 . The result is shown in Figure 2 by
 246 a thick gray line. Visual inspection of the fit quality and the value of the corresponding merit function indicate that
 247 the approximation of the measured function of m by a linear combination of two functions coming exclusively from
 248 leakage-matrix analysis is perfectly adequate. The inferred ratio $\sigma_h^2/\sigma_r^2 = 9.6 \pm 0.1$ indicates that horizontal velocities
 249 in the turbulent flow are about 3 times bigger than vertical velocities. The fit quality remains adequate when the
 250 same analysis is applied to data at a smaller degrees ℓ . An interesting observation is that the measured ratio σ_h^2/σ_r^2
 251 increases monotonically to 18.2 ± 0.5 at $\ell = 100$ and 20.5 ± 2.9 at $\ell = 5$. At degree $\ell < 5$, this measurement loses
 252 stability due to an insufficient number of the available orders m . This finding may indicate that bigger convective cells
 253 have a bigger average ratio of horizontal to vertical velocities.

Another finding is that the observed m -averaged value $\overline{B}^2(\omega)$ stays nearly constant in the entire degree range: it drops monotonically when going from $\ell = 0$ to $\ell = 300$, but only by about 15 percent. For comparison, in medium- ℓ SOHO MDI measurements of much smaller spatial resolution, this variation amounts to two orders of magnitude. This behavior indicates that in the degree range $\ell \leq 300$, the spatial resolution of the HMI instrument is indeed almost perfect. To clarify this point, our analysis can be made independent of the leakage-matrix computations—assuming, of course, that the spatial resolution of the instrument is perfect.

In addition to the coordinate system (θ, φ) with the z -axis aligned with the solar rotation axis, we introduce another coordinate system (θ', φ') with the z' -axis (from which θ' is counted) directed from the Sun towards the observer. Considering the projection of the turbulent velocity field $\mathbf{v}(\theta, \varphi, t)$ (Equation 1) on the CCD plane directly, without its decomposition in vector spherical harmonics, we have

$$B_{\ell m}^2(\omega) = \text{E} \left| \int_{4\pi} Y_{\ell m}^*(\theta, \varphi) \Pi(\sin \theta') \hat{z}' \cdot \tilde{\mathbf{v}}(\theta, \varphi, \omega) d\varpi \right|^2, \quad (24)$$

where $\tilde{\mathbf{v}}(\theta, \varphi, \omega)$ is the Fourier transform of $\mathbf{v}(\theta, \varphi, t)$ at frequency shifted by advection effects, and $\Pi(\sin \theta')$ is an apodization function, $\sin \theta'$ being the radial coordinate in the image plane in units of the apparent solar radius. Evaluating the measure of the stochastic signal in the way described in Section 2 gives immediately

$$B_{\ell m}^2(\omega) = \int_{4\pi} Y_{\ell m}^*(\theta, \varphi) Y_{\ell m}(\theta, \varphi) \Pi^2(\sin \theta') \left[\cos^2 \theta' \sigma_r^2(\omega) + \frac{1}{2} \sin^2 \theta' \sigma_h^2(\omega) \right] d\varpi, \quad (25)$$

where $\cos^2 \theta'$ and $\sin^2 \theta'/2$ account for the line-of-sight projection effects. Using an addition theorem for spherical harmonics, the m -averaged value is

$$\overline{B}^2(\omega) = \frac{1}{2\ell + 1} \sum_{m=-\ell}^{\ell} B_{\ell m}^2(\omega) = \frac{1}{4\pi} \int_{4\pi} \Pi^2(\sin \theta') \left[\cos^2 \theta' \sigma_r^2(\omega) + \frac{1}{2} \sin^2 \theta' \sigma_h^2(\omega) \right] d\varpi, \quad (26)$$

a result which does not depend on the target degree ℓ .

By expanding $\cos^2 \theta' \Pi^2(\sin \theta')$ and $\sin^2 \theta' \Pi^2(\sin \theta')$ in Equation (25) in spherical harmonics and transforming the result to (θ, φ) -coordinates, it is also possible to evaluate the right-hand side at individual m -values. We skip the details of this analysis, as its principal motivation was to check the accuracy of our leakage-matrix computations. The numerical results of the two approaches turned out to be the same.

The slight variation of the apparent values of $\overline{B}^2(\omega)$ with degree ℓ indicates that the leakage matrices can be improved by setting the PSF width to a small but non-zero value. We conclude that the measurements of the solar noise can be used to calibrate the effective PSF of the instrument. This option may be particularly interesting for analyzing data obtained with SOHO MDI instrument.

4. TEMPORAL DOMAIN

We can de-rotate the power spectra by frequency shifting them according to the results of the differential rotation measurement. The m -average of the de-rotated spectra in the entire frequency domain of SDO HMI data at $\ell = 300$ is shown in Figure 3.

At frequencies less than about $200\mu\text{Hz}$, the variation of the observed power with ℓ and m cannot be explained by our model, which loses its ability to fit the data with any reasonable accuracy. In this spatiotemporal domain, our assumption of negligibly small correlation length is violated by supergranular-scale convective motions, as seen in Doppler-velocity power as a function of m and ω , shown on a gray scale in Figure 4. The well-defined ridge at $m > 0$ (prograde waves) is produced by the rotation of the solar supergranulation pattern. A small but noticeable curvature of the ridge is due to faster rotation of the equatorial regions. At frequencies less than about $50\mu\text{Hz}$, the observed power drops rapidly because of the de-trending applied to the timeseries of spherical harmonic components.

In this study, the data analysis was limited to frequencies below the oscillation resonances. We can hope that the dependence of the noise power on ℓ and m (the $B_{\ell}^2(m)$) measured in this frequency range will stay the same at higher frequencies; this assumption, of course, remains to be verified by addressing residuals of spectral fitting procedures. We note that at frequencies from about 3 mHz and higher, the measurement of the background component

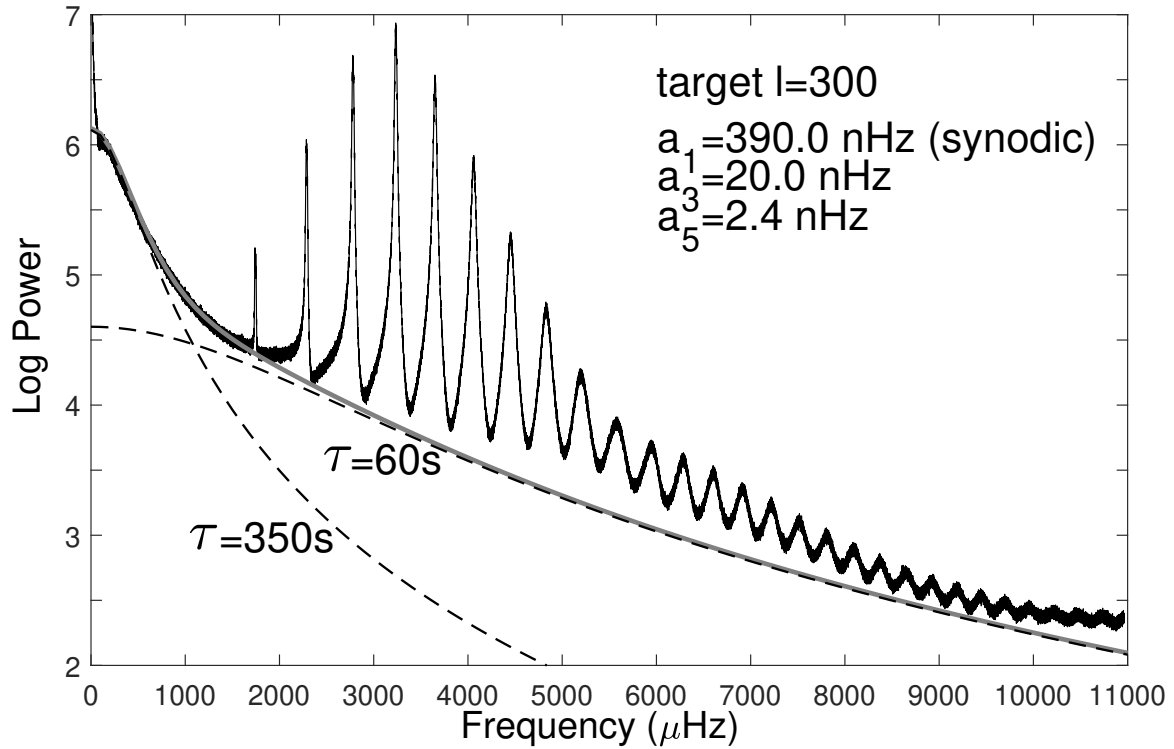


Figure 3. De-rotated and m -averaged SDO HMI power spectrum at $l = 300$ (thin line). Dashed lines show two simple models (see text); their sum is shown by the thick gray line.

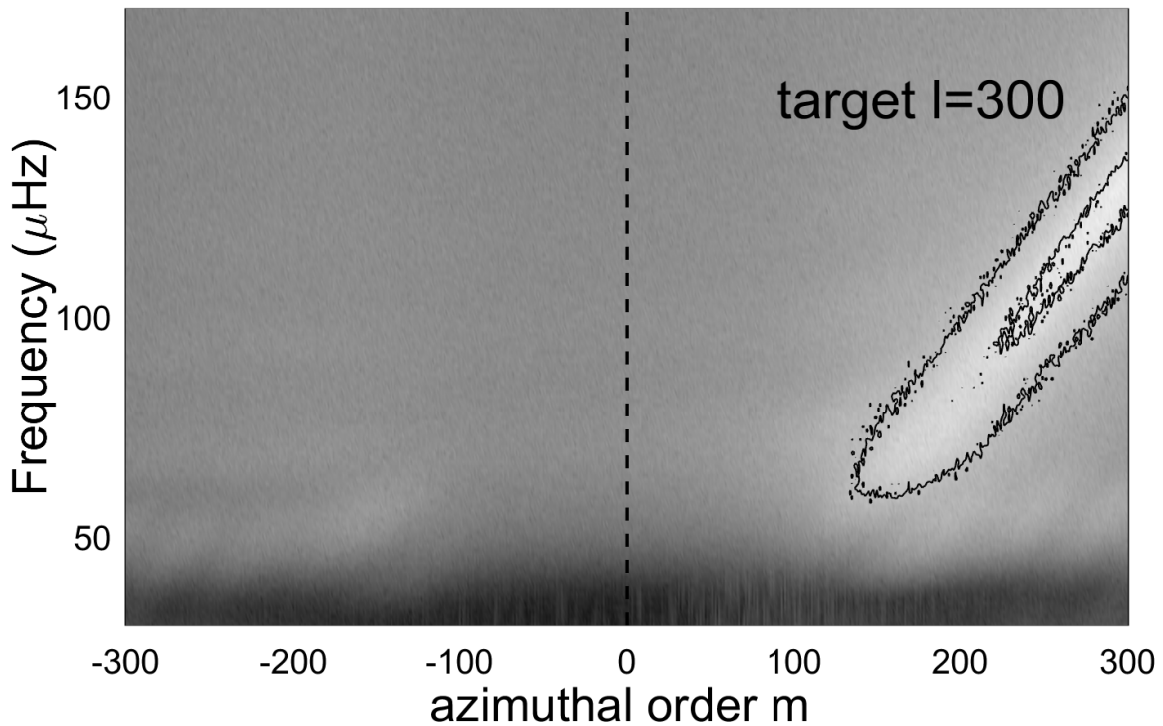


Figure 4. Velocity power at $\ell = 300$ and frequencies below $170 \mu\text{Hz}$.

is difficult because the signal-to-noise ratio of acoustic resonances becomes very high. At these frequencies, it is now the uncorrelated background which gets buried below the resonant power.

We suggest a simple model for the frequency dependence of the background noise $\overline{B}^2(\omega)$ to be used as an initial guess in the mode-fitting procedures. Imagine a convective eddy emerging on the solar surface from below at time $t = 0$. Let the observed velocity increase linearly with time and then drop exponentially:

$$v = \begin{cases} 0, & t < 0 \\ \frac{t}{\tau^2} e^{-\frac{t}{\tau}}, & t \geq 0. \end{cases} \quad (27)$$

Taking the Fourier transform, the observed power is $(1 + \omega^2 \tau^2)^{-2}$. The Fourier power is a cosine Fourier transform of the autocorrelation function, which is

$$ACF = \frac{1}{4\tau} \left(1 + \left| \frac{t}{\tau} \right| \right) e^{-|\frac{t}{\tau}|}. \quad (28)$$

We adjust a linear combination of these 'seismic events' with two different values of τ to approximate the expected variation of the uncorrelated background in the entire frequency range; the result is shown in Figure 3 by two dashed lines for the two separate components and by the thick gray line for their sum. The fitted values of τ , about 6 minutes and 1 minute, are of the order of the lifetimes of solar granules and shorter. A relative excess of observational power at the highest frequencies may be due to an aliasing signal coming from frequencies higher than the Nyquist frequency.

5. DISCUSSION

Implementation of our model in frequency measurements is relatively straightforward. At each degree, ℓ , the even functions $B_\ell^2(m)$ are measured from the de-rotated power spectra around some frequency below all the detectable resonances. The initial approximation for the frequency dependence of the uncorrelated background $\overline{B}^2(\omega)$ is then improved by fitting individual multiplets in the power spectra. When the instrument's resolution is imperfect, as with SOHO MDI measurements or those of high degree ℓ from SDO HMI, the more minor sensitivity to modes of higher degree ℓ will be captured in $B_\ell^2(m)$.

The suggested measurement of differential rotation from power spectra at frequencies below acoustic resonances should be undertaken with more data of lower and higher degrees ℓ analyzed in different frequency intervals. It would be interesting to extend these measurements to datasets obtained at different times to explore temporal variations of the subsurface differential rotation, also known as 'torsional oscillations'.

In our limited exercise with observational data, we have another finding which deserves more extensive data analysis. The inferred ratio of magnitudes of horizontal and vertical components of convective velocities σ_h^2/σ_r^2 clearly tends to get bigger when ℓ gets smaller; it indicates that in bigger convective cells, horizontal velocities become more dominant.

Our model becomes inconsistent with observations at frequencies below $200\mu\text{Hz}$, since our basic assumption of small correlation length breaks down when observations are affected by signals from supergranular convective cells. Here, we enter the spatiotemporal domain targeted by [Beck & Schou \(2000\)](#) in their encouraging measurements of differential rotation of solar supergranulation pattern from Dopplergrams provided by the SOHO MDI instrument. An approach which is more sophisticated than ours is needed to deal with turbulent-velocity correlations simultaneously in both space and time.

We thank Jesper Schou and an anonymous referee for multiple useful comments and suggestions. HMI is an instrument on board the Solar Dynamic Observatory (SDO), and the data used for this work are courtesy of the NASA/ SDO and the HMI science team.

APPENDIX

The leakage matrices used in this study were calculated using the semi-analytic approach described in ([Vorontsov & Jefferies 2005](#)). This approach was extended in ([Vorontsov & Jefferies 2013](#)) to account explicitly for non-zero solar B-angle (**the heliographic latitude of the central point of the solar disk**). In this study, we need to develop the analysis further to include the instrument's response to components of the velocity field described by toroidal vector spherical harmonics. We have also noticed an inaccuracy in the earlier treatment of the B-angle

effect: line-of-sight projection was done in the direction orthogonal to the solar rotation axis, thus missing the observer. Therefore, we outline the overall algorithm briefly, adding proper extensions.

We implement three separate leakage matrices— $R_{\ell'\ell}^{m'm}$, $H_{\ell'\ell}^{m'm}$ and $T_{\ell'\ell}^{m'm}$, with response coefficients to the vertical component of poloidal vector fields, to their horizontal component, and to the toroidal vector fields, respectively. We discard here all possible instrumental and optical distortions.

We choose the coordinate system (r, θ, φ) such that its z -axis is aligned with solar rotation, axis y is orthogonal to the line of sight, and axis x (from which φ is measured) is directed towards the observer when solar B-angle is zero. We choose another axis z' , which points toward the observer. The angle β between z to z' is 90 degrees minus the solar B-angle. We start with a line-of-sight projection of the vector velocity fields, allowing further analysis to work with scalar fields. The projection of vector \mathbf{v} onto the line of sight is

$$\hat{z}' \cdot \mathbf{v} = \sin \beta \hat{x} \cdot \mathbf{v} + \cos \beta \hat{z} \cdot \mathbf{v}. \quad (1)$$

For poloidal vector fields, we need an expansion in spherical harmonics of $\hat{x} \cdot \hat{r} Y_{\ell m}(\theta, \varphi)$, $\hat{z} \cdot \hat{r} Y_{\ell m}(\theta, \varphi)$, $\hat{x} \cdot \nabla_1 Y_{\ell m}(\theta, \varphi)$, and $\hat{z} \cdot \nabla_1 Y_{\ell m}(\theta, \varphi)$. These decompositions are (Vorontsov & Jefferies 2005):

$$\begin{aligned} \hat{x} \cdot \hat{r} Y_{\ell m}(\theta, \varphi) &= -\frac{1}{2} \left[\frac{(\ell+m-1)(\ell+m)}{(2\ell-1)(2\ell+1)} \right]^{\frac{1}{2}} Y_{\ell-1, m-1}(\theta, \varphi) + \frac{1}{2} \left[\frac{(\ell-m-1)(\ell-m)}{(2\ell-1)(2\ell+1)} \right]^{\frac{1}{2}} Y_{\ell-1, m+1}(\theta, \varphi) \\ &+ \frac{1}{2} \left[\frac{(\ell-m+1)(\ell-m+2)}{(2\ell+1)(2\ell+3)} \right]^{\frac{1}{2}} Y_{\ell+1, m-1}(\theta, \varphi) - \frac{1}{2} \left[\frac{(\ell+m+1)(\ell+m+2)}{(2\ell+1)(2\ell+3)} \right]^{\frac{1}{2}} Y_{\ell+1, m+1}(\theta, \varphi), \quad (2) \end{aligned}$$

$$\hat{z} \cdot \hat{r} Y_{\ell m}(\theta, \varphi) = \left[\frac{(\ell+m)(\ell-m)}{(2\ell-1)(2\ell+1)} \right]^{\frac{1}{2}} Y_{\ell-1, m}(\theta, \varphi) + \left[\frac{(\ell+m+1)(\ell-m+1)}{(2\ell+1)(2\ell+3)} \right]^{\frac{1}{2}} Y_{\ell+1, m}(\theta, \varphi), \quad (3)$$

$$\begin{aligned} \hat{x} \cdot \nabla_1 Y_{\ell m}(\theta, \varphi) &= -\frac{\ell+1}{2} \left[\frac{(\ell+m-1)(\ell+m)}{(2\ell-1)(2\ell+1)} \right]^{\frac{1}{2}} Y_{\ell-1, m-1}(\theta, \varphi) + \frac{\ell+1}{2} \left[\frac{(\ell-m-1)(\ell-m)}{(2\ell-1)(2\ell+1)} \right]^{\frac{1}{2}} Y_{\ell-1, m+1}(\theta, \varphi) \\ &- \frac{\ell}{2} \left[\frac{(\ell-m+1)(\ell-m+2)}{(2\ell+1)(2\ell+3)} \right]^{\frac{1}{2}} Y_{\ell+1, m-1}(\theta, \varphi) + \frac{\ell}{2} \left[\frac{(\ell+m+1)(\ell+m+2)}{(2\ell+1)(2\ell+3)} \right]^{\frac{1}{2}} Y_{\ell+1, m+1}(\theta, \varphi), \quad (4) \end{aligned}$$

$$\hat{z} \cdot \nabla_1 Y_{\ell m}(\theta, \varphi) = (\ell+1) \left[\frac{(\ell+m)(\ell-m)}{(2\ell-1)(2\ell+1)} \right]^{\frac{1}{2}} Y_{\ell-1, m}(\theta, \varphi) - \ell \left[\frac{(\ell+m+1)(\ell-m+1)}{(2\ell+1)(2\ell+3)} \right]^{\frac{1}{2}} Y_{\ell+1, m}(\theta, \varphi). \quad (5)$$

Corresponding expressions for toroidal vector spherical harmonics are derived in the same way; the result is

$$\hat{x} \cdot [-\hat{r} \times \nabla_1 Y_{\ell m}(\theta, \varphi)] = -\frac{i}{2} [(\ell+m)(\ell-m+1)]^{\frac{1}{2}} Y_{\ell, m-1}(\theta, \varphi) - \frac{i}{2} [(\ell-m)(\ell+m+1)]^{\frac{1}{2}} Y_{\ell, m+1}(\theta, \varphi), \quad (6)$$

$$\hat{z} \cdot [-\hat{r} \times \nabla_1 Y_{\ell m}(\theta, \varphi)] = -im Y_{\ell, m}(\theta, \varphi). \quad (7)$$

The rest of the analysis is the same as in (Vorontsov & Jefferies 2005, 2013): we rotate the coordinate system by angle β to direct the z axis towards the observer, convolve the image with the PSF in the apodization domain, and rotate the coordinate system back to its original orientation. Symmetry relations for the resulting leakage matrices are

$$\begin{aligned} R_{\ell'\ell}^{-m', -m}(\beta) &= (-1)^{m'+m} R_{\ell'\ell}^{m'm}(\beta), \quad H_{\ell'\ell}^{-m', -m}(\beta) = (-1)^{m'+m} H_{\ell'\ell}^{m'm}(\beta), \\ T_{\ell'\ell}^{-m', -m}(\beta) &= (-1)^{m'+m+1} T_{\ell'\ell}^{m'm}(\beta), \end{aligned} \quad (8)$$

$$\begin{aligned} R_{\ell'\ell}^{m', m}(\pi - \beta) &= (-1)^{\ell'+\ell+m'+m} R_{\ell'\ell}^{m'm}(\beta), \quad H_{\ell'\ell}^{m', m}(\pi - \beta) = (-1)^{\ell'+\ell+m'+m} H_{\ell'\ell}^{m'm}(\beta), \\ T_{\ell'\ell}^{m', m}(\pi - \beta) &= (-1)^{\ell'+\ell+m'+m+1} T_{\ell'\ell}^{m'm}(\beta). \end{aligned} \quad (9)$$

Matrices R and H , which specify the instrumental response to poloidal vector fields, are real; matrix T is imaginary. Equation (9) shows that for poloidal fields (which describe undistorted eigenfunctions of solar oscillations) the amplitudes of the response coefficients of the instrument are identically zero when the solar B -angle is zero and $\ell' + \ell + m' + m$

377 is odd; we refer to these leaks as 'prohibited' leaks. For toroidal fields, situation is reversed: prohibited leaks are those
 378 with $\ell' + \ell + m' + m$ even. For prohibited leaks, the leak amplitude is an odd function of the solar B -angle; for
 379 unprohibited leaks, it is even function of B . In power spectra, the magnitude of spatial leaks (the absolute value of
 380 leak amplitude squared) is always an even function of the solar B -angle, i.e. does not depend on its sign.

REFERENCES

- 381 Beck, J. G., & Schou, J., 2000, *Solar Phys.*, 193, 333
 382 Fleck, B., Couvidat, S., Straus, T., 2011, *Solar Phys.*, 271,
 383 27
 384 Korzennik, S. G., 2005, *ApJ*, 626, 585
 385 Korzennik, S. G., 2023, *Frontiers in Astron. & Space Sci.*,
 386 9, id.1031313
 387 Larson, T. P., & Schou, J., 2015, *Solar Phys.*, 290, 3221
 388 Larson, T. P., & Schou, J., 2018, *Solar Phys.*, 293, 29
 389 Ritzwoller, M. H., & Lavelly, E. M., 1991, *ApJ*, 369, 557
 390 Schou, J., Christensen-Dalsgaard, J., Thompson, M. J.,
 391 1994, *ApJ*, 433, 389
 392 Snodgrass, H. B., & Ulrich, R. K., 1990, *ApJ*, 351, 309
 393 Vorontsov, S. V. 2007, *MNRAS*, 378, 1499
 394 Vorontsov, S. V., & Jefferies, S. M., 2005, *ApJ*, 623, 1202
 395 Vorontsov, S. V., & Jefferies, S. M., 2013, *ApJ*, 778, 75
 396 Vorontsov, S. V., Christensen-Dalsgaard, J., Schou, J.,
 397 Strakhov, V. N., Thompson, M. J., 2002, in: *From Solar*
 398 *Min to Max: Half a Solar Cycle with SOHO*, ed. A.
 399 Wilson, *Proc. SOHO 11 Symposium* (ESA SP-508;
 400 Noordwijk: ESA), 111